Force Pattern Characterization of *C. elegans* in Motion

Ali Ghanbari*[1], Volker Nock*[2], Wenhui Wang[1], Richard Blaikie[2], J. Geoffrey Chase[1], XiaoQi Chen[1], and Christopher E. Hann[1]
[1]Mechanical Engineering, University of Canterbury, Christchurch 8140, NEW ZEALAND
[2]MacDiarmid Institute, University of Canterbury, Christchurch 8140, NEW ZEALAND
Email: wenhui.wang@canterbury.ac.nz

***Abstract* - *C. elegans* is a worm that could be mutated to have different muscle arms, which may generate distinct force patterns when the worm moves. In this paper, an integrated system employing both a novel PDMS device and a visual feedback from the device is reported. The silicone elastomer-based PDMS device consists of arrays of pillars, which forms open channels for the worm to move in and bend the pillars in contact. Enabled by a single vision sensor (CCD/CMOS camera), the computer vision system is able to transform the forces generated by *C. elegans*, through detecting the deflection of the pillars with sub-pixel accuracy. The experimental results demonstrate that the current vision-based force sensing system is capable of performing robust force measurements at a full 30 Hz with a 1.52 μN resolution. The framework has the potential to significantly facilitate the study on the relationship between muscle arms and force patterns of *C. elegans* in motion, and thus gives a better understanding of muscle arms development and modeling.**

I. INTRODUCTION

C. elegans is a multicellular eukaryotic nematode living in temperate soil environments. Due to its relative simplicity in anatomy, *C. elegans* has been used extensively as a model organism for studies on cellular differentiation, neural networking and genetic modification in eukaryotes [1]. It was the first multicellular organism to have its genome completely sequence [2].

Commonly in biological study, the worm *C. elegans* can be genetically modified to obtain mutants with different number of muscle arms, which in turn affects the motion patterns of the nematode. It is of biologists' particular interest to study the correlation between muscle arms and motion patterns. For example, to determine if there is a positive relationship such that a mutant with more muscle arms generates greater motion forces. As the worm is tiny (~1 mm in length and < 100 μm in width, invisible to the naked eye), the typical dynamic sensors used in millimeter and larger scales cannot be used to measure the force existing.

Most existing force measurement techniques are designed for using with biological cells. At the micro–nanoscale, measurements are often conducted using MEMS (micro-electro-mechanical systems) transducers, such as capacitive force sensors [3- 5] and piezoresistive cantilevers [6, 7]. Compared to other cellular force measurement techniques, such as optical tweezers [8], atomic force microscopy (AFM) [9], magnetic bead measurement [10] and micropipette aspiration [11], MEMS force sensors are more cost-effective and provide flexibility for system integration. However, the construction of MEMS force transducers typically depends on silicon micromachining which requires sophisticated equipment sets and an increase in processing effort. Significant care must also be taken in properly designing and shielding electronic detection circuits in order to obtain a satisfactory force measurement resolution. Furthermore, issues such as biocompatibility and operating in an aqueous environment for *C. elegans* to survive, often pose stringent challenges and intricacies in MEMS design, material selection, and microfabrication.

Two decades ago, the flexible substrate method was introduced for characterizing mechanical interactions between biological cells and their surrounding environment [12]. More recently, an innovative approach employing microfabricated PDMS (polydimethylsiloxane) post/pillar structures as force transducers was reported to visually measure traction forces generated by adherent cells (smooth muscle cells [13], epithelial cells [14], and cardiac myocytes [15]). Unlike flexible thin substrates, the post/pillar structures do not require heavily complex computations for calculating traction forces. Compared to silicon-based MEMS devices, PDMS-based devices are biocompatible and can be readily constructed using the soft lithography technique [16, 17] without requiring intensive microfabrication efforts or sophisticated equipment sets.

Inspired by the previous work [18], this paper reports a PDMS device and the image processing method capable of characterizing the force pattern of *C. elegans* in motion. To measure the force, the worm is put inside the open channel formed by parallel arrays of pillars on the PDMS device. When moving in a sinusoidal manner, the worm bends the pillars, whose deflection can be sensed by a camera. Figure 1 shows the schematic of *C. elegans* movement in the PDMS device and the corresponding bending the pillars. Using a well-established force-deflection model of the pillars, the force of *C. elegans* in motion can be resolved from the deflection obtained via image processing.

* *Shared first authorship*

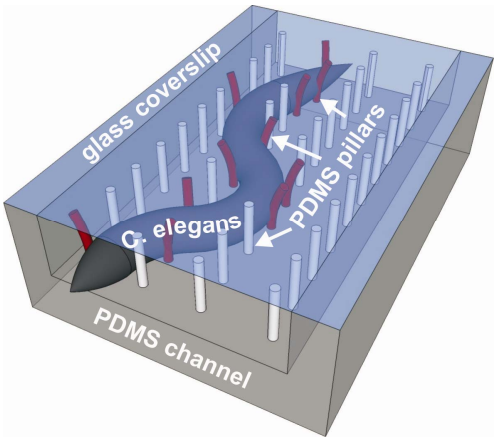

Figure 1. Schematic of the *C.elegans* movement in the PDMS device.

II. Device Fabrication and Experimental Data Collection

A. Device Fabrication

For this research, force measurement devices were fabricated by replica-molding of a photoresist master in polydimethylsiloxane (PDMS, Sylgard 184, Dow Corning) silicone polymer [19]. Figure 2 shows a schematic of the device fabrication process. First, a master mold was formed in SU-8 negative photoresist (MicroChem) on a 4" silicon wafer as substrate. In brief, an initial layer of SU-8 2025 was spin-coated to a thickness of 15 µm, softbaked according to the resist datasheet and exposed in a Suess MA6 mask aligner using a high resolution chrome mask to form the channel outline [20]. After postbake, a second, 100 µm thick layer of SU-8 2100 was coated on top of the first layer. The wafer was softbaked again and exposed through a second mask containing both the channel outline and pillar array. Finally, the resist pattern was developed in (1-methoxy-2-propyl) acetate in an ultra-sonic bath, rinsed with IPA and hardbaked for 20 min at 150°C.

For replica-molding, PDMS pre-polymer was prepared by mixing Sylgard 184 base:curing agent in a 10:1 w/w ratio. The pre-polymer was thoroughly mixed and degassed to remove any air bubbles. Meanwhile, the surface of the SU-8 mold was treated by exposure to trimethylchlorsilane (TMCS, Sigma Aldrich) vapor for 10 min to facilitate de-molding. Following this step, the mixture was poured onto the mold and degassed again to allow for bubble-free filling of the pillar holes. The mold was then placed on a hotplate and cured for 1 h at 80°C. After cooling to room temperature, the replica was carefully peeled off and cured for a further 3 hrs at 150°C. Individual devices were cut out using a scalpel and placed on microscope slides for handling.

B. C. elegans Culture

Nematodes were cultured as described in [1]. 60 mm Nematode Growth Medium (NGM) Petri dishes are prepared for holding the worm. 600 µl of saturated LB culture of bacteria *E. coli* strain OP50 was spread onto the fresh NGM agar plate for feeding the worm. The dishes were allowed to dry for 1 hour before use.

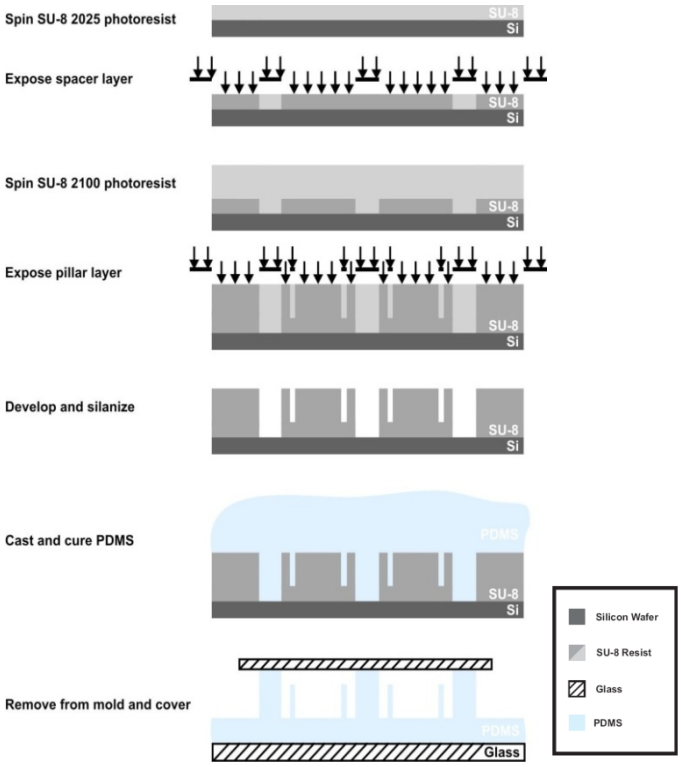

Figure 2. Schematic of the device fabrication.

C. Device Loading

Prior to introduction of *C. elegans,* the surface of the PDMS device was rendered hydrophilic by use of a laboratory corona treater (Electro-Technic Products). The top of the device was then covered with a 22x22 mm glass coverslip (ESCO) to enclose the pillar-containing part of the channel. Following this, de-ionized water (DI) was dispensed onto the uncovered inlet by pipette and the channel structure was filled via capillary action. Individual *C. elegans* were transferred from the culture dish by use of an inoculating needle and carefully placed in the water-filled channel inlet. A thin water layer was thus formed on the device surface to provide a moisturized environment that is required for the worm to move normally.

D. Data Collection

Worm movement was imaged using a Nikon Eclipse 80i fluorescence microscope in bright field mode. A digital camera (DS-5Mc, Nikon) was used to record still images and movies for analysis on a PC. Images were post-processed to determine pillar deflection vectors and then infer the forces.

III. Vision-Based Force Measurement

A. Force Calculation

Figure 3 shows photograph of the PDMS force measurement device. In this device the height and diameter of pillars were 100 µm and 40 µm respectively and the inter-pillars distance was 60 µm.

To calculate the force imposed by the *C. elegans* on the pillars, the relationship between pillars deflection and force has to be derived. It was observed that the worms tended to move at almost half of the pillars height while swimming in de-ionized water. Therefore, it is assumed the worm touches the pillars at half of their height. Thus, in the force model derivation, it is assumed the force had been imposed on the pillars at a height of 50 µm.

The ratio of half pillar height (50 µm) to diameter (40 µm) does not satisfy the pure bending assumption of linear elastic beams, which presumes that at the place of force, the height to diameter ratio must be greater than 5. Thus, both bending and shear must be considered to map the deflection to the applied force at touch point [21]. Therefore, the displacement at this point can be derived:

$$\delta = \left(\frac{l^3}{3EI} + \frac{20(1+\gamma)l}{9AE}\right).f \quad (1)$$

where f is the force, l and A are the pillar half height and cross-section area, I is the moment of inertia, and E and γ are Young's modulus and Poisson's ratio. The Poisson ratio for PDMS is 0.5 [22].

From the point of applied force to the free end of the pillar, the displacement will be linear because no other force exists. Therefore, this displacement can be derived based only on bending:

$$\delta' = \frac{l^2}{2EI}(h-l).f \quad (2)$$

Here, h is the pillar height. Thus, the force can be calculated as follows:

$$f = \frac{\Delta}{\left(\frac{l^3}{3EI}+\frac{20(1+\gamma)l}{9AE}\right)+\frac{l^2}{2EI}(h-l)} \quad (3)$$

, where

$$\Delta = \delta + \delta' \quad (4)$$

Pillar diameters are considered uniform along the height (Figure 3 d). Therefore, the moment of inertia of each pillar is defined:

$$I = \frac{\pi D^4}{64} \quad (5)$$

Note that drag forces on the pillars by the fluidic environment are safely ignored [23].

In Equation 3 the only unknown parameters are Young's modulus E, and pillar deflection Δ. Based on the PDMS device fabrication specifications, E is equal to 1.6 MPa [24]. Hence, the force imposed by *C. elegans* can be obtained by measuring the pillars deflection Δ, which is detectable via image processing discussed in the following section.

B. Image Processing and Deflection Measurement

An image processing algorithm was developed and adapted to track pillar deflection accurately. A total of 35 consecutive frames were selected for processing. Without loss of generality, three specific pillars (Figure 4) were selected for showing the deflection measurement.

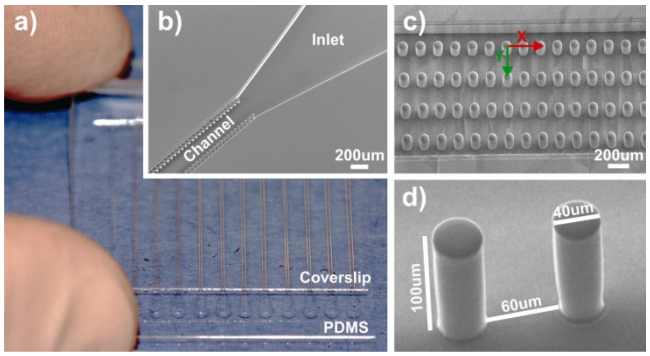

Figure 3. a) Photograph of the PDMS force measurement device incorporating multiple channels with different pillar dimensions and spacings. A glass coverslip was used to cover the channel area while the inlet structure remained open. b) SEM micrograph depicting the inlet structure of a channel (coverslip removed for imaging). c) SEM micrograph of the channel area.

Both dual and quadruple arrays of pillars were fabricated. d) SEM close-up of a pair of round PDMS pillars with diameter 40µm. Pillar height was kept constant at 100µm while X and Y spacings were varied from 20 to 60 µm and 150 to 300 µm, respectively, for different channels.

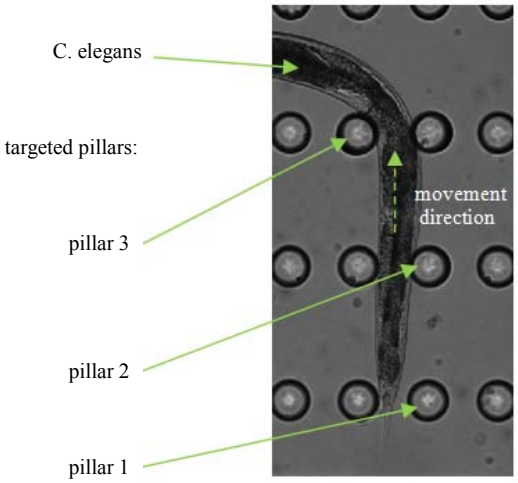

Figure 4. Top view of targeted pillars for deflection measurement and *C. elegans* movement direction.

First, frames were converted to black and white to have binary images for subsequent extraction of the edge coordinates, as shown in Figure 5 (a). Second, three zones were defined to extract each pillar image in an assigned square window. Then, the following algorithm was applied to trace the outline of the outer circle of the deflected pillar:

- Scanning the square window from bottom left until a nonzero pixel belonging to the outer circle of the pillar from the top view is found. Pixel P_0 is a starting pixel of the circle tracing.
- Defining the tracing direction
- Searching the 3×3 neighborhood of the current pixel in an anti-clockwise direction, beginning the

neighborhood search in the pixel positioned in the defined tracing direction. The first nonzero pixel found is the second circle point P_1.

- The circle point tracing is repeated up to detecting nth pixel P_n.

Figure 5 (b) shows a traced outline of the outer circle of the three targeted pillars for n=65 points.

A least-square fitting algorithm was employed to fit a circle to the traced points. The algorithm minimizes the following equation, which is the sum of squares of algebraic distance of the n detected points from the circle center:

$$G(x_c, y_c, r) = \sum_{i=1}^{n}[(x_i - x_c)^2 + (y_i - y_c)^2 - r^2]^2 \qquad (6)$$

Here, x_c and y_c are the coordinates of the circle center and r is the circle radius. First, define:

$$A = -2x_c \qquad (7)$$

$$B = -2y_c \qquad (8)$$

$$C = x_c^2 + y_c^2 - r^2 \qquad (9)$$

Equation 6 can thus be rewritten:

$$G(A, B, C) = \sum_{i=1}^{n}(x_i^2 + y_i^2 Ax_i + Bxy_i + C)^2 \qquad (10)$$

The result is a differentiating equation with respect to A, B and C that creates a linear equation set. By solving this equation set, center coordinates and a radius are calculated. Figure 6 shows the fitted circles for three targeted pillars. Figure 7 shows processed square windows of three pillars and fitted circles in six different frames. In all 35 processed frames the fitted circles accurately locate the top view of deflected pillars including their centers for tracking.

IV. Results and Discussion

Visually measured deflections were substituted into the pillar-mechanics model (Equation 3) to calculate imposed forces corresponding to each frame. Figure 8 shows the measured force vs. frame. In all processed frames, *C. elegans* is touching pillar 2. This indicates that the force on pillar 2 is always larger than zero. Figure 9 demonstrates the linear relationship between deflection vs. force. As this figure shows, the maximum deflection is 20.36 µm, experienced by pillar 2. This number over pillar height (100 µm) is small enough to satisfy that the small-deflection assumption of linear elasticity holds [21]. Therefore, we have a valid linear relation of force and deflection as derived in Equation 3. Figure 10 shows the resulting forces in the x and y coordinate directions. As this figure illustrates, for all three pillars, the force magnitude in x direction is higher than y direction. This complies with the *C. elegans* movement direction, which is *vertically* bottom to top, and therefore hits the pillars in x direction. At the same time, when *C. elegans* tries to turn *horizontally*, pillars exhibit an additional deflection in y direction. Figure 10 indicates that this

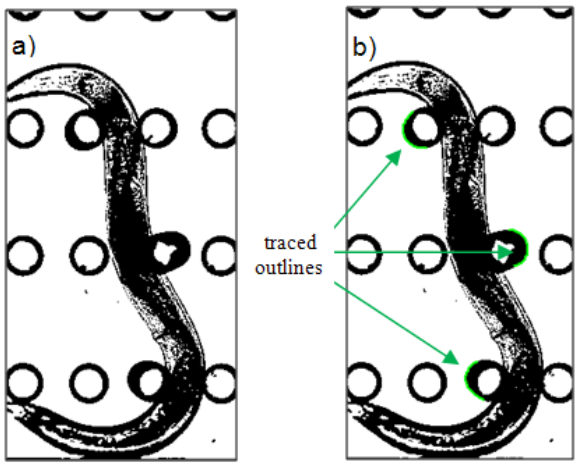

Figure 5. a) Converted binary image. b) Traced outlines of the outer circles.

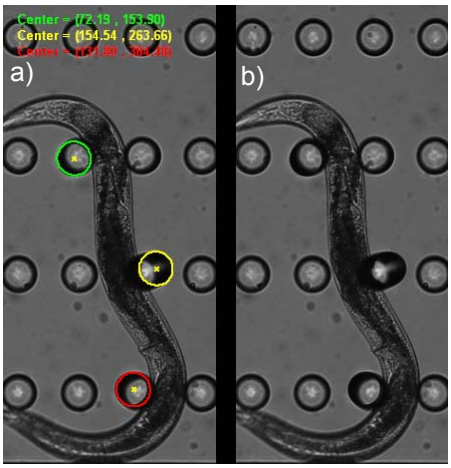

Figure 6. a) Processed image: fitted circles for three pillars as well as circles centers locating. b) Original image.

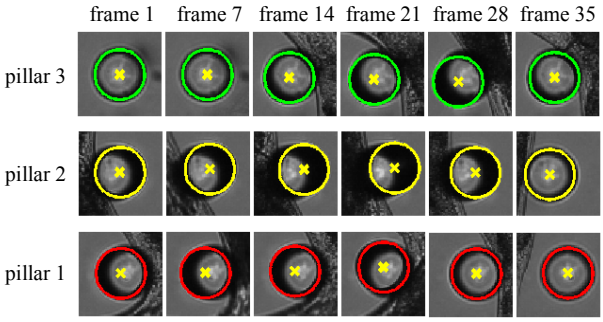

Figure 7. Processed square windows for 3 targeted pillars and fitted circles

TABLE I
Maximum forces imposed by the *C. elegans* to the three pillars of interest

	Pillar 1	**Pillar 2**	**Pillar 3**
max | f_x | (µN)	17.93	31.85	17.48
max | f_y | (µN)	6.58	11.52	10.08
max | f | (µN)	18.15	33.87	19.76

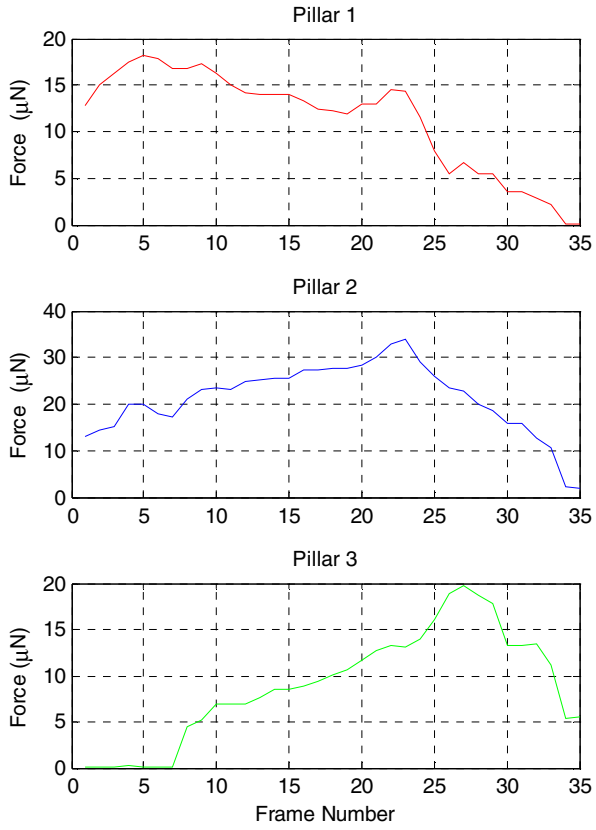

Figure 8. Force magnitudes for the three pillars of interest.

latter force is smaller at all times. Table I. shows the maximum absolute value of force received by three pillars in x and y coordinate directions and in total ($\vec{F} = \vec{F_x} + \vec{F_y}$). In this study, the maximum calculated force was 33.87 μN when pillar 2 experienced its maximum deflection of 20.36 μm.

Figure 11 demonstrates the cumulative distribution of calculated forces (for all forces in three pillars except zero forces). Sorting the forces (smallest to largest) and distributing them between 0 to 1 with steps of one over the number of sorted forces, a nearly linear cumulative distribution function (CDF) can be obtained, which implies an approximately uniform distribution of forces. This result shows a highly variable and continuous force level produced by the worm, which is in accordance with biological results and the anatomy of *C. elegans.*

Currently, the data was collected by manually moving a stage to follow the motion of the worm. This is cumbersome as the worm is very active. Therefore, future work will include integrating the previously developed real-time automatic *C. elegans* tracking system [25], which employs a micromanipulator to track a moving worm and keeps it in the field of view of the camera. This way, long-term force pattern analysis will be possible. Additionally, more biological experiment will be conducted to collect statistically meaningful data for large-scale samples (up to 200 worms). Force patterns

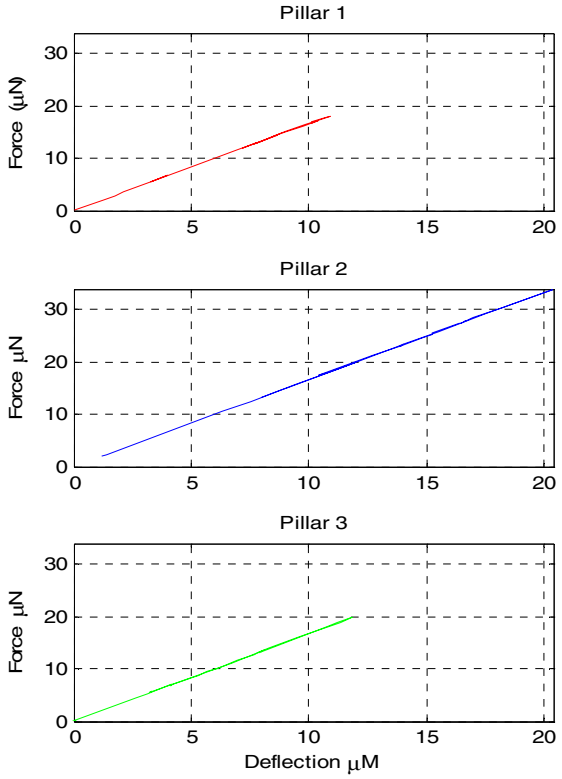

Figure 9. Pillars deflection vs. force

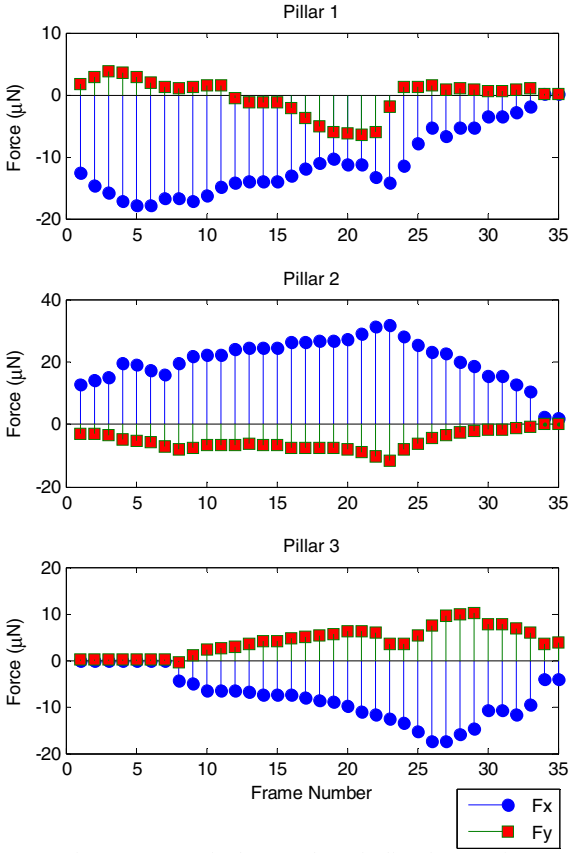

Figure 10. Force in the x- and y-axis directions vs. frame.

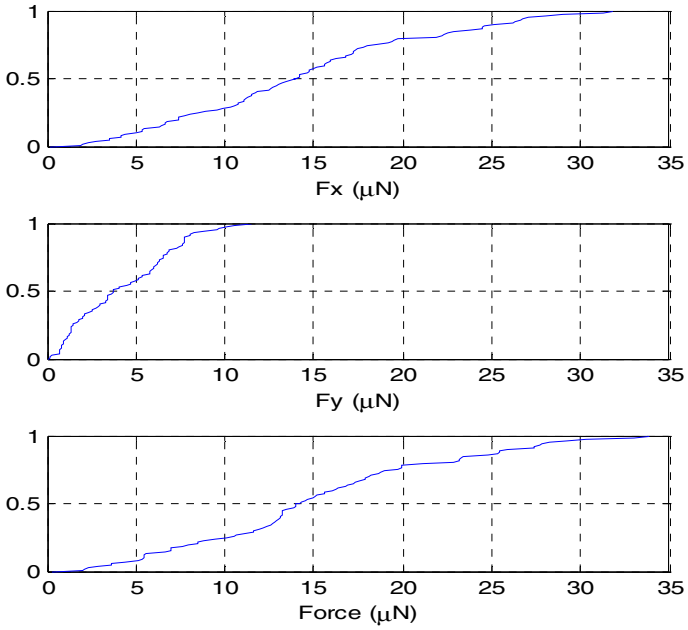

Figure 11. Cumulative distribution of calculated forces

for various motion patterns of a worm will be obtained, such as turning, foraging, and forwarding/backwarding.

V. CONCLUSIONS

This paper, proposes, develops and presents the initial application of a method to measure *C. elegans* force by using a microfabricated PDMS device and an image processing algorithm to infer forces from measured deflections. The image processing algorithm was shown to accurately detect the deflected pillar top circle view and track its center. Employing the derived mechanics model of the deflected pillars enables the force to be inferred. The maximum measured *C. elegans* force applied to the pillars was 33.87 μN for an observed deflection of 20.36 μm. The measured deflections and calculated forces provide very useful information about the forces and patterns generated by *C. elegans* in motion. Analysis of the forces generated shows that *C. elegans* modulates its force levels across a continuum, based on the direction of movement or resistance experienced, which matches biological observations of muscle having continuous force output spectrum.

ACKNOWLEDGMENT

The authors would like to thank Craig Galilee for providing the *C. elegans* and Helen Devereux for technical assistance.

REFERENCES

[1] S. Brenner, *The Genetics of Caenorhabditis Elegans Genetics*, vol. 77, pp. 71-94, May 1974.

[2] T. C. e. S. Consortium, "Genome Sequence of the Nematode C. elegans: A Platform for Investigating Biology," Science, vol. 282, pp. 2012-2018, December 1998.

[3] Y. Sun, K. T. Wan, B. J. Nelson, J. Bischof and K. Roberts, Mechanical property characterization of the mouse zona pellucida *IEEE Trans. NanoBioSci.* vol.2 pp.279–86 2003.

[4] Y. Sun Y and B. J. Nelson, Biological cell injection using an autonomous microrobotic system, *Int. J. Robot. Res 2002.*

[5] Y. Sun, S N Fry, D P Potassek, D J Bell and B J Nelson, Characterizing fruit fly flight behaviour using a microforce sensor with a new comb drive configuration, J. Microelectromech. Syst. vol.14 pp. 4–11, 2005.

[6] G Lin, G Palmer, K S J Pister and K P Roos, Miniature heart cell force transducer system implemented in MEMS technology *IEEE Trans. Biomed. Eng.* vol.9 996–1006, 2001.

[7] M E Fauver, D L Dunaway, D H Lillenfeld, H G Craighead and G H Pollack, Microfabricated cantilevers for measurement of subcellular and molecular forces *IEEE Trans. Biomed. Eng.* vol.45 pp.891–8, 1998.

[8] J Conia, B S Edwards and S Voelkel, The micro-robotic laboratory: optical trapping and scissing for the biologist, *J. Clin. Lab. Anal.* vol.11 pp.28–38, 1997.

[9] G T Charras, P P Lehenkari and M A Horton, Atomic force microscopy can be set to mechanically stimulate osteoblasts and evaluate cellular strain distribution, *Ultramicroscopy vol* 86, pp. 85–95 , 2001.

[10] J N Fass and D J Odde, Tensile force dependent neurite elicitation via Anti-β1 integrin antibody-coated magnetic beads, *Biophys. J. vol.* 85 pp. 623–36, 2003.

[11] R M Hochmuth, Micropipette aspiration of living cells, *J. Biomech vol. 33 pp. 15-22* 2000.

[12] A K Harris, P Wild and D Stopak, Silicone rubber substrata: a new wrinkle in the study of cell locomotion, *Science vol 208 pp.* 177–9, 1980.

[13] J. L. Tan, J. Tien, D. M .Pirone, D. S. Gary, K Bhadriraju and C S Chen , Cells lying on a bed of microneedles: an approach to isolate mechanical force, *Proc. Natl Acad. Sci. USA,* vol.100, pp.1484–9, 2003.

[14] O D Roure, A Saez, A Buguin, R H Austin, P Chavrier, P Siberzan and B Ladoux, Force mapping in epithelial cell migration, *Proc. Natl Acad. Sci. USA,* vol.102 pp.2390–2395, 2005.

[15] Y. Zhao and X. Zhang, Cellular mechanics study in cardiac myocytes using PDMS pillars array, *Sensors Actuators,* vol. 125, pp. 398–404, 2006.

[16] Y. Xia, E. Kim, X. M. Zhao, J A Rogers, M Prentiss and G M Whitesides, Complex optical surfaces formed by replica molding against elastomeric masters, *Science,* vol. 273, pp. 347-349, 1996.

[17] E. Kim, Y. Xia and G M Whitesides Polymer microstructures formed by moulding in capillaries, *Nature,* vol. 376 pp. 581–4, 1995.

[18] X. Y. Liu, Y. Sun, W. H. Wang, and B. M. Lansdorp, Vision-based cellular force measurement using an elastic microfabricated device, *J. of Micromechanics and Microengineering*, 17(7), pp. 1281-1288, 2007.

[19] Y. N. Xia and G. M. Whitesides, "Soft lithography," Angewandte Chemie-International Edition, vol. 37, pp. 551-575, March 1998.

[20] MicroChem, SU-8 2000 Datasheet, 2008.

[21] A. C. Ugural and S. K. Fenster *Advanced Strength and Applied Elasticity*, NY: McGraw-Hill, 2003.

[22] J. E. Mark *Polymer Data Handbook*, Oxford: Oxford University Press

[23] W. F. Hughes and J. A. Brighton *Schaums's Outline of Theory and Problems of Fluid Dynamics*, NY: McGraw-Hill, 1999.

[24] F. Schneider, T. Fellner, J. Wilde and U. Wallrabe, " Mechanical properties of silicones for MEMS", *J. of Micromechanics and Microengineering,* vol. 18, pp.1-9, 2008.

[25] W. H. Wang, Y. Sun, S. J. Dixon, M. Alexander, and P. J. Roy, A micropositioning system with real-time feature extraction capability for quantifying *C. elegans* locomotive behavior, *IEEE Conference on Automation Science and Engineering (CASE2007)*, Scottsdale, Arizona, Sep. 22-25, 2007.